Microwave Chip-Based Beam Splitter for Low-Energy Guided Electrons

Jakob Hammer,* Sebastian Thomas, Philipp Weber, and Peter Hommelhoff
Department für Physik, Friedrich-Alexander-Universität Erlangen-Nürnberg, Staudtstraße 1, 91058 Erlangen, Germany
(Received 12 August 2014; published 23 June 2015)

We present a novel beam splitter for low-energy electrons using a micro-structured guiding potential created above the surface of a planar microwave chip. Beam splitting arises from smoothly transforming the transverse guiding potential for an electron beam from a single-well harmonic confinement into a double well, thereby generating two separated output beams with 5 mm lateral spacing. Efficient beam splitting is observed for electron kinetic energies up to 3 eV, in excellent agreement with particle tracking simulations. We discuss prospects of this novel beam splitter approach for electron-based quantum matter-wave optics experiments.

DOI: 10.1103/PhysRevLett.114.254801 PACS numbers: 41.85.-p, 37.10.Ty, 84.40.Az

A beam splitter is the quintessential component in many modern physics experiments. The visualization of the quantum mechanical phase hinges on it. Its various realizations have enabled the observation of fundamental physics phenomena such as quantum optics experiments with photons [1], many-body interference experiments with cold atoms in optical lattices [2], neutron interferometry [3], and fundamental interference studies with heavy molecules [4]. Prominent among these studies are interference experiments with electrons, which have enabled groundbreaking insight into, for example, the wave-particle duality with massive particles [5–8] and the Aharanov-Bohm effect [9].

A plethora of electron interferometry experiments [10] was triggered by the invention of the electrostatic biprism in 1955 [11]. It is a relatively rugged transverse beam splitting element that also serves as a workhorse in modern commercial electron microscopes employing holographic techniques [12,13]. In particular, interference experiments with low-energy electrons have demonstrated reduced radiation damage allowing the nondestructive imaging of biological molecules [14].

An entirely new electron optical toolkit arises from the manipulation of slow electrons in free space using a microwave quadrupole guide [15]. The generation of the necessary high-frequency electric fields by means of a planar microwave chip provides ease of scalability and the flexibility to engineer versatile guiding potentials in the near field of the microwave excitation. This renders surface-electrode structures ideally suited for the implementation of electron beam splitters or resonators with prospects for novel quantum optics experiments with guided electrons. Based on a similar technology, surface-electrode ion traps have been employed to provide finely structured potential landscapes. For example, junctions for trapped ions have been realized [16–21], or double-well potentials with small distances between the potential minima to couple separately trapped ions via the Coulomb force [22,23]. In this Letter, we show the concept and the experimental demonstration of a new beam splitter for guided electrons with kinetic energies in the electron-volt range.

Oscillating electric fields allow the generation of a time-averaged restoring force to confine the motion of charged particles in free space [24]. The microwave guide for electrons is based on a two-dimensional, high-frequency quadrupole potential providing transverse confinement, similar to a linear Paul trap [25]. The details of this concept are summarized in the Supplemental Material [26]. The stable operation of the guide practically requires oscillation frequencies of the microwave drive in the gigahertz range. The resulting tight transverse confinement is described by a time-averaged, harmonic pseudopotential. Moreover, electrons can be confined in the saddle point of any inhomogeneous high-frequency electric potential $\phi(\vec{r}, t) = \phi_{RF}(\vec{r})\cos(\Omega t)$ with drive frequency Ω if the potential gradient is nearly constant over the range of the electron's oscillation [24]. We generate such an electric potential by means of a planar microwave chip. As a key feature, this chip-based technology provides the unique possibility to achieve high field gradients in the near field of a micro-structured electrode design allowing for precise control over the motion of the guided electrons.

For the on-chip splitting of the guided electron beam we incorporate a junction in the guiding potential by gradually transforming the driving electric field from a quadrupole to a hexapole symmetry along the chip. Using hexapole electric fields a junction can be realized in the pseudopotential [33]. Figure 1(a) illustrates electric field line plots in the transverse xz plane at three locations along the planar electrode structure. Additionally, an isopotential surface of the guiding potential at 0.25 meV is shown, with microwave drive parameters as given below. The electric field line plots and the isopotential surface plot have been obtained by simulating the electric field that is created by the surface electrodes, the design of which is shown in Fig. 1(b) [34]. The microwave signal is applied to the red

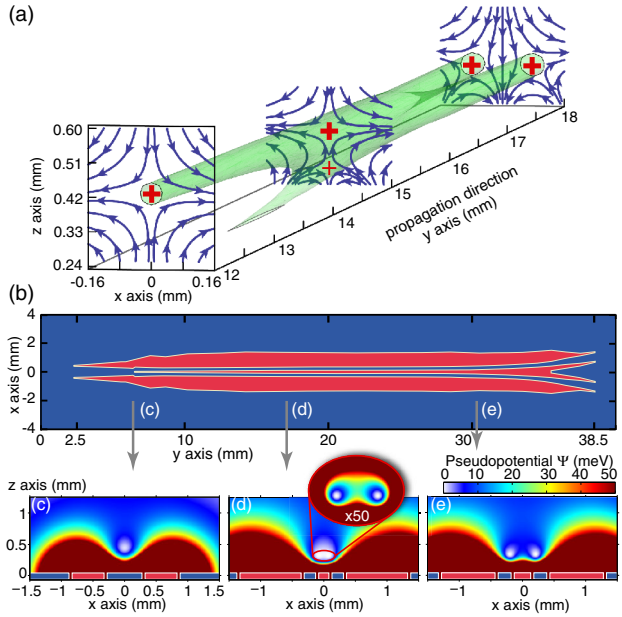

FIG. 1 (color online). Electrode design of the planar beam splitter chip and pseudopotential simulations. (a) Electric field line plots together with an isopotential surface of the guiding potential at 0.25 meV. (b) Numerically optimized chip electrodes with microwave signal applied to the red electrodes. The remaining blue area is grounded. By means of the tapered central electrode the transition from a quadrupole to a hexapole electric field symmetry is achieved, as shown in (a). (c) Cut through the electrode plane at $y = 6.5$ mm showing the simulated pseudopotential in the transverse plane. The pseudopotential minimum forms at a height of 450 μm above the substrate providing harmonic confinement. (d) At $y = 17$ mm the additional central electrode, with a width of 160 μm, results in the formation of a double-well pseudopotential with a separation of 150 μm between the minima. A fourfold magnified zoom in is shown in the inset with a 50 times amplified color code. By increasing the width of the center electrode the separation of the double-well minima is gradually increased. (e) At $y = 30$ mm the central electrode is 260 μm wide, leading to a separation of the minima of 400 μm.

electrodes, whereas the ground plane is indicated in blue. At a position of $y = 12$ mm along the chip, the electric field in the transverse plane is governed by a strong quadrupole component leading to the creation of a saddle point guiding electrons in the center, as indicated by the red cross. By changing the width of the tapered signal electrode in the center, the electric field above the guiding chip can be transformed along the y direction from a quadrupole to a hexapole symmetry. The hexapole field component gives rise to an additional saddle point that continuously approaches the guiding potential minimum from the chip surface. This is indicated in the field line plot at $y = 15$ mm, where two saddle points form on the vertical z axis. Further along the chip, for increasing y, both saddle points merge in the xz plane and subsequently separate in the transverse x direction.

An electric field with a predominant quadrupole component may be generated by five electrodes on a planar chip substrate [35]. Figure 1(c) shows a cut through the electrode structure at $y = 6.5$ mm together with a simulation of the pseudopotential in the xz plane. As a result of the strong quadrupole component, a single guiding potential minimum forms at a height of 450 μm above the chip surface. The simulation is performed with a microwave drive frequency $\Omega = 2\pi \times 990$ MHz and a voltage amplitude $V_0 = 16$ V on the signal electrodes. Figure 1(d) shows a cut through the electrode plane further along the chip at $y = 17$ mm. Here it comprises seven electrodes with a microwave signal electrode in the center. This leads to the creation of a strong hexapole field component giving rise to a double well in the pseudopotential. By adjusting the width of the central electrode, the separation of the double-well minima can be controlled. The distance between them is 150 μm in Fig. 1(d) and 400 μm in Fig. 1(e), which shows the simulated pseudopotential at $y = 30$ mm. The barrier height between the wells is 0.5 meV at $y = 17$ mm and 11.5 meV at $y = 30$ mm.

We have numerically optimized the electrode layout of the microwave chip using the SURFACE PATTERN package [36–38]. The hexapole symmetry of the electric field close to the intersection point results in a junction with two incoming and two outgoing channels. By means of a systematic variation of the shape of the chip electrodes, we have reduced distortions in the beam splitter potential that arise from the additional incoming channel and minimized its impact on the trajectories of guided electrons. Details are given in the Supplemental Material [26].

The microwave signal is delivered to the signal electrodes [drawn in red in Fig. 1(a)] by a coplanar waveguide structure on the backside of the chip (not shown), which is interconnected to the top side by laser-machined, plated through holes (see the Supplemental Material [26] for details). The experiments are performed with $\Omega = 2\pi \times$ 990 MHz and an on-chip microwave power of 4.3 W, which results in $V_0 \approx 16$ V [39].

A home-built thermionic electron gun [40] provides an electron beam with kinetic energies down to 1 eV and beam currents on the order of several 10 femtoamperes. As a result of this low electron current, electron-electron interaction effects are irrelevant. The beam is collimated using two apertures resulting in a full opening angle of 14 mrad and a spot diameter of about 100 μm at the guide entrance. Behind the microwave chip, electrons are detected on a microchannel plate electron detector [41] after traveling 10 mm in free space. Images of the phosphor screen behind the microchannel plate are recorded by a CCD camera [42].

Figure 2(a) shows the detector signal recorded for an electron kinetic energy of 1.5 eV and the microwave parameters given above. We observe an electron signal with two symmetrically split up components. The distance between the two main spots is 5 mm, whereas each spot has

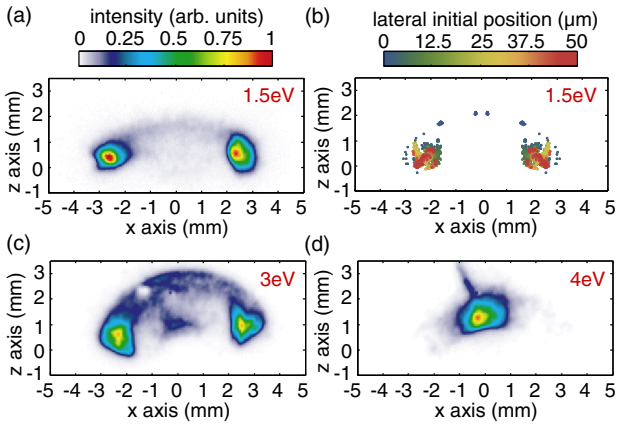

FIG. 2 (color online). Experimental (a) and simulated (b) detector signal of the split electron beam with $E_{\mathrm{kin}} = 1.5$ eV. (a) Clearly two guided beams are visible containing 80% of all detected electrons. A faint signal of lost electrons is detected between the guided electron spots (between $x = -1.5$ and 1.5 mm). The color scale depicts the intensity of the raw CCD image. (b) Simulated beam splitter signal based on trajectory simulations. All signatures including the position and size of the output beams and the electron loss are reproduced by the simulation. The color scale corresponds to the initial lateral displacement of the electron trajectories along x. See text for details. The dependence of the detected electron signal on the kinetic energy is shown for 3 eV (c) and 4 eV (d). For 4 eV the beam splitting potential is too weak to split up the beam.

an average full-width at half-maximum diameter of 0.75 mm. Additionally, a faint signal of lost electrons is detected between the two guided components. The guided electrons comprise 80% of the detected signal. Clearly, the injected electron beam is split into two collimated output beams.

In order to fully understand the observed features, we perform classical particle tracking simulations. We release electron trajectories from a disk with a diameter of 100 μm and propagate them numerically in the simulated electric field of the beam splitter chip. Figure 2(b) shows the resulting simulated electron signal, which is in excellent agreement with the experimentally observed output signal. The color scale illustrates the initial lateral displacement of the electrons along the x axis. Evidently, electrons released closest to the symmetry axis of the beam splitter potential [blue dots in Fig. 2(b)] are preferentially lost. This can be understood by considering the extreme case of an electron being released at $x = 0$ mm. Because of the planar symmetry of the beam splitter potential in the x direction, such a classical trajectory does not encounter any transverse potential gradient and therefore no deflecting force along x. As a result, this trajectory cannot follow the pseudopotential minimum paths of the separating double well and is only deflected vertically away from the substrate. For this reason, electrons that propagate closest to the symmetry axis may preferentially become lost from the beam splitter potential. Using quantum mechanical simulations we show in the Supplemental Material [26] that *lossless*, adiabatic splitting of an electron beam can be achieved by means of an optimized beam splitter potential.

Further, we have varied the electron kinetic energy from 1.5 eV to 3 eV. We find that the signal of lost electrons becomes larger with energy as depicted in Fig. 2(c) as compared to Fig. 2(a). This is because with the increasing forward momentum of the electrons, the transverse gradient of the beam splitter potential becomes insufficient to significantly deflect the electrons in the lateral x direction. Accordingly, the electron trajectories cannot follow the separating paths of the potential minimum and are lost from the potential. As a consequence, for energies above 4 eV we observe no splitting anymore and all electrons are detected around $x = 0$ mm in Fig. 2(d).

The beam diameter of 100 μm, attained with the thermionic electron gun, is not matched to the diameter of the quantum mechanical ground state wave function (on the order of 100 nm) of the transverse beam splitter potential. As a result, we estimate that the guided electrons fill up the potential up to energies of 0.75 meV in the current experiment, which is orders of magnitude larger than the quantum ground state energy on the order of 0.1 μeV. Therefore, the experiment is well described by classical particle tracking simulations. However, the direct injection of electrons into low-lying motional quantum states should be possible by matching the incoming electron beam to the ground state wave function of the transverse guiding potential [43].

Ultimately, the wave-optical propagation of a guided electron is governed by discretized motional quantum states of the transverse guiding potential. In the following, we illustrate the properties of the microwave beam splitter quantum mechanically and discuss prospects for electron-based quantum optics experiments.

It is instructive to compare the microwave beam splitter for electrons to a typical *amplitude* beam splitter as used in light optics. As detailed above, the beam splitter potential based on a hexapole intersection features two incoming and two outgoing channels. For simplicity we consider a planar symmetry of the beam splitter potential around the intersection point along y, as indicated in Fig. 3(a). We label an incoming electron that occupies the motional ground state of the left (right) arm of the beam splitter with the state $|L\rangle$ ($|R\rangle$). To understand the evolution of these localized input states, one needs to consider the transverse energy eigenstates $|1\rangle$ and $|2\rangle$ at different points along the length of the beam splitter [see the insets of Fig. 3(a)]. While the paths are spatially well separated by a potential barrier, these are the symmetric and antisymmetric ground states of a double-well potential, and their energy is (almost) degenerate. The localized input states are a superposition $|L\rangle = (|1\rangle + |2\rangle)/\sqrt{2}$ and $|R\rangle = (|1\rangle - |2\rangle)/\sqrt{2}$ of these eigenstates.

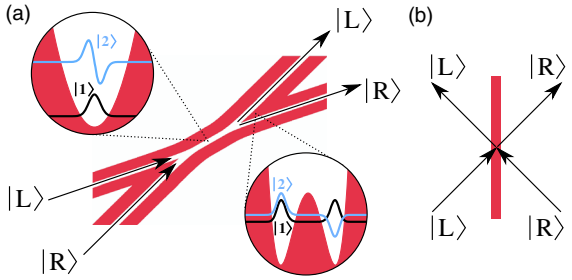

FIG. 3 (color online). Sketch of an adiabatic microwave beam splitter (a) in comparison to a typical amplitude beam splitter as used in light optics (b).

As $|L\rangle$ and $|R\rangle$ are not energy eigenstates, electrons will, in principle, tunnel between these two states. However, as long as the potential barrier is much larger than the transverse energy of these states, both wells are separated and the tunneling frequency is negligibly low. From a quantum mechanical point of view, the function of the beam splitter is to increase this frequency by bringing the two wells closer together and eventually merging them. In the center part of the splitter, the superposition states $|L\rangle$ and $|R\rangle$ are then no longer spatially separated and, hence, the wave amplitude is transferred between $|L\rangle$ and $|R\rangle$. In general, an incoming state with amplitudes l in the left and r in the right path is turned to an outgoing state with amplitudes l' and r'. If we describe the left path by the state $|L\rangle = \binom{1}{0}$ and the right path by the state $|R\rangle = \binom{0}{1}$, the effect of the beam splitter B can be described as a multiplication of the state with a unitary matrix: $\binom{l'}{r'} = B\binom{l}{r}$. If we disregard phase shifts, B is essentially a rotation matrix whose angle depends on the oscillation frequency ω between $|L\rangle$ and $|R\rangle$ and the time the electron spends in the center part of the splitter.

The previous discussion assumes that the electron initially occupies the motional ground state of the transverse guiding potential. As described above, this can be achieved using a diffraction-limited electron gun in order to match the injected electron beam to the ground state wave function of the guiding potential. Interestingly, a multimode interferometer using higher vibrational states has been investigated in the context of guided atom interferometry [44]. Furthermore, the above description requires that an electron initially prepared in the quantum ground state maintains its state while propagating along the beam splitter. The current design lacks this crucial feature of adiabaticity. Using quantum mechanical simulations we have investigated the key prerequisites to achieve adiabatic splitting of the ground state mode. The details of the simulations are described in the Supplemental Material [26]. The amount of transverse vibrational excitations depends critically on the geometric opening angle between the beam splitter paths as well as the energy separation of the transverse eigenstates. As one would expect, a smooth splitting process and, hence, a small opening angle is beneficial. By scaling the guiding potential transversely, we find that the half opening angle of the current design has to be reduced from 40 to 0.1 mrad. In addition, we have to increase the microwave drive frequency to $\Omega = 2\pi \times 8$ GHz to obtain beam splitting with 90% of the population remaining in the ground state mode after the splitting. The eightfold higher Ω effectively increases the curvature of the transverse potential and results in an $\sqrt{8}$-fold larger energy level separation of the single-well potential of $\Delta E \sim 0.24\ \mu$eV and, hence, an oscillation frequency $\omega = \Delta E/\hbar \sim 2\pi \times 58$ MHz. Both the small beam splitter angle and the higher Ω require a redesign of the current microwave chip.

As just introduced, beam splitters used in quantum optics experiments [like in Fig. 3(b)] are usually described by unitary matrices, which reflect the coupling between the amplitudes of two states [45,46]. The microwave beam splitter demonstrated here is a promising new technology because it may become such an *amplitude* beam splitter for electrons. Most current experiments on electron interference rely on the electrostatic biprism, which is a *wave front* beam splitter. The wave front beam splitter can be regarded as an electron optical device that generates two virtual sources by a spatial division of the beam. In that case, interference between both output beams relies on the spatial coherence of the electron source [47]. In contrast, using an amplitude splitter, the phase between both output beams and their amplitudes are fully determined by the physical properties of the beam splitter device. To this end, the manipulation of electrons using the microwave beam splitter augments the already available, rich electron optical toolkit and may herald new quantum optics experiments with free electrons. In particular, a novel quantum electron microscopy concept is emerging that employs multiple *amplitude* splittings of a quantum particle's wave function for the noninvasive imaging of biological samples [48,49].

We thank J. Hoffrogge, J. McNeur, P. Kruit, and the QEM Collaboration for discussions. This research is funded by the Gordon and Betty Moore Foundation.

*jakob.hammer@fau.de

[1] L. Mandel and E. Wolf, *Optical Coherence and Quantum Optics* (Cambridge University Press, Cambridge, 1995).
[2] I. Bloch, J. Dalibard, and W. Zwerger, Rev. Mod. Phys. **80**, 885 (2008).
[3] H. Rauch and S. Werner, *Neutron Interferometry* (Oxford University Press, New York, 2000).
[4] T. Juffmann, A. Milic, M. Müllneritsch, P. Asenbaum, A. Tsukernik, J. Tüxen, M. Mayor, O. Cheshnovsky, and M. Arndt, Nat. Nanotechnol. **7**, 297 (2012).
[5] C. Davisson and L. H. Germer, Phys. Rev. **30**, 705 (1927).
[6] H. Boersch, Phys. Z. **44**, 202 (1943).

[7] L. Marton, J. A. Simpson, and J. A. Suddeth, Phys. Rev. **90**, 490 (1953).
[8] A. Tonomura, J. Endo, T. Matsuda, T. Kawasaki, and H. Ezawa, Am. J. Phys. **57**, 117 (1989).
[9] A. Tonomura, N. Osakabe, T. Matsuda, T. Kawasaki, J. Endo, S. Yano, and H. Yamada, Phys. Rev. Lett. **56**, 792 (1986).
[10] F. Hasselbach, Rep. Prog. Phys. **73**, 016101 (2010).
[11] G. Möllenstedt and H. Düker, Naturwissenschaften **42**, 41 (1955).
[12] D. Gabor, Nature (London) **161**, 777 (1948).
[13] A. Tonomura, *Electron Holography* (Springer, Heidelberg, 1999).
[14] M. Germann, T. Latychevskaia, C. Escher, and H.-W. Fink, Phys. Rev. Lett. **104**, 095501 (2010).
[15] J. Hoffrogge, R. Fröhlich, M. A. Kasevich, and P. Hommelhoff, Phys. Rev. Lett. **106**, 193001 (2011).
[16] J. M. Amini, H. Uys, J. H. Wesenberg, S. Seidelin, J. Britton, J. J. Bollinger, D. Leibfried, C. Ospelkaus, A. P. VanDevender, and D. J. Wineland, New J. Phys. **12**, 033031 (2010).
[17] D. L. Moehring, C. Highstrete, D. Stick, K. M. Fortier, R. Haltli, C. Tigges, and M. G. Blain, New J. Phys. **13**, 075018 (2011).
[18] G. Shu, G. Vittorini, A. Buikema, C. S. Nichols, C. Volin, D. Stick, and K. R. Brown, Phys. Rev. A **89**, 062308 (2014).
[19] C. E. Pearson, D. R. Leibrandt, W. S. Bakr, W. J. Mallard, K. R. Brown, and I. L. Chuang, Phys. Rev. A **73**, 032307 (2006).
[20] K. Wright *et al.*, New J. Phys. **15**, 033004 (2013).
[21] W. K. Hensinger, S. Olmschenk, D. Stick, D. Hucul, M. Yeo, M. Acton, L. Deslauriers, C. Monroe, and J. Rabchuk *et al.*, Appl. Phys. Lett. **88**, 034101 (2006).
[22] K. R. Brown, C. Ospelkaus, Y. Colombe, A. C. Wilson, D. Leibfried, and D. J. Wineland, Nature (London) **471**, 196 (2011).
[23] M. Harlander, R. Lechner, M. Brownnutt, R. Blatt, and W. Hänsel, Nature (London) **471**, 200 (2011).
[24] F. G. Major, V. N. Gheorghe, and G. Werth, *Charged Particle Traps* (Springer, Heidelberg, 2005).
[25] W. Paul, Rev. Mod. Phys. **62**, 531 (1990).
[26] See Supplemental Material at http://link.aps.org/supplemental/10.1103/PhysRevLett.114.254801, which includes Refs. [27–32], for details on the working principle and the experimental realization of the microwave beam splitter. Furthermore, quantum mechanical simulations are presented taking into account electron matter-wave propagation along the beam splitter.
[27] D. M. Pozar, *Microwave Engineering*, 3rd ed. (John Wiley, New York, 2005).
[28] W. Hänsel, J. Reichel, P. Hommelhoff, and T. W. Hänsch, Phys. Rev. A **64**, 063607 (2001).
[29] V. Jelic and F. Marsiglio, Eur. J. Phys. **33**, 1651 (2012).
[30] J. Hoffrogge and P. Hommelhoff, New J. Phys. **13**, 095012 (2011).
[31] J. A. Fleck, J. R. Morris, and M. D. Feit, Appl. Phys. **10**, 129 (1976).
[32] M. Feit, J. Fleck, and A. Steiger, J. Comp. Physiol. **47**, 412 (1982).
[33] J. H. Wesenberg, Phys. Rev. A **79**, 013416 (2009).
[34] P. Hommelhoff and J. Hammer, Patent pending, Patent No. PCT/EP2014/001784 (2014).
[35] J. H. Wesenberg, Phys. Rev. A **78**, 063410 (2008).
[36] See http://atom.physik.unibas.ch/people/romanschmied/code/SurfacePattern.php.
[37] R. Schmied, New J. Phys. **12**, 023038 (2010).
[38] R. Schmied, J. H. Wesenberg, and D. Leibfried, Phys. Rev. Lett. **102**, 233002 (2009).
[39] A standing microwave signal is established as their wavelength, $\lambda = 200$ mm, is much larger than the electrode length, $L = 38$ mm.
[40] P. W. Erdman and E. C. Zipf, Rev. Sci. Instrum. **53**, 225 (1982).
[41] Photonis, Model No. APD 2 PS 40/12/10/12 46:1 P20.
[42] The Imaging Source, Model No. DMK 41AU02.
[43] J. Hammer, J. Hoffrogge, S. Heinrich, and P. Hommelhoff, Phys. Rev. Applied **2**, 044015 (2014).
[44] E. Andersson, T. Calarco, R. Folman, M. Andersson, B. Hessmo, and J. Schmiedmayer, Phys. Rev. Lett. **88**, 100401 (2002).
[45] A. Zeilinger, Am. J. Phys. **49**, 882 (1981).
[46] W. P. Schleich, *Quantum Optics in Phase Space* (Wiley-VCH, Berlin, 2005).
[47] M. Born and E. Wolf, *Principles of Optics*, 7th ed. (Cambridge University Press, 1999).
[48] W. P. Putnam and M. F. Yanik, Phys. Rev. A **80**, 040902 (2009).
[49] S. Thomas, C. Kohstall, P. Kruit, and P. Hommelhoff, Phys. Rev. A **90**, 053840 (2014).